



Cite this: RSC Adv., 2019, 9, 32594

 Received 21st August 2019
 Accepted 7th October 2019

 DOI: 10.1039/c9ra06562h
rsc.li/rsc-advances

Mechanism and kinetics of the atmospheric reaction of 1,3,5-trimethylbenzene bicyclic peroxy radical with OH[†]

 Xiaoxiao Lin,^a Zhenli Yang,^{ab} Hui Yu,^{ab} Yanbo Gai  ^{*a} and Weijun Zhang ^{*a}

The bicyclic peroxy radical (BPR) is the key intermediate during atmospheric oxidation of aromatics. In this paper, the reaction mechanisms and kinetics of the atmospheric reaction of the 1,3,5-trimethylbenzene (1,3,5-TMB) BPR with the OH radical were studied by density functional theory (DFT) and conventional transition-state theory (CTST) calculations. The product channels of formation of the 1,3,5-TMB trioxide (ROOOH), OH-adducts and Criegee intermediate (CI) have been identified, and the geometries and energies of all the stationary points were calculated at the M08-HX/6-311 + g(2df,2p) level of theory. In addition, the rate constants for the individual reaction pathway at 298 K were calculated. The results showed that OH addition reactions including the formation of ROOOH and OH-adducts are the main pathways, whereas Criegee intermediate formation is of minor importance.

1. Introduction

Aromatics constitute an important fraction (20–40%) of the total non-methane hydrocarbons (NMHCs) in the urban atmosphere which are mostly emitted by fuel combustion and industrial solvent evaporation.^{1–3} 1,3,5-Trimethylbenzene is a significant component of the suite of aromatic hydrocarbons that leads to the production of tropospheric ozone and secondary organic aerosols (SOA).⁴ Atmospheric oxidation of 1,3,5-trimethylbenzene is mainly initiated by the OH radical, and the bicyclic peroxy radical (BPR) is the key intermediate during the oxidation.⁵ The detailed gas-phase chemical processes including the degradation mechanism of 1,3,5-trimethylbenzene can be described by MCMv3.1 which is the Master Chemical Mechanism version 3.1. As shown in Scheme 1, in the OH-initiated oxidation of 1,3,5-trimethylbenzene (TMB), the yields of the initial products formed after the OH addition to the aromatic ring in MCMv3.1 are 0.79 for the 1,3,5-TMB bicyclic peroxy radical (BPR) which have been detected experimentally.^{4,6}

The main chemical fate of the bicyclic peroxy radical (BPR) depends on levels of NO_x (NO_x = NO₂ + NO). The major pathway is the reaction with NO in polluted urban areas, which is responsible for tropospheric ozone production.⁷ While in low NO_x conditions, the reaction with HO₂ or with other peroxy

radicals plays a larger role.^{8,9} Recently, the reaction with OH radicals in clean environments has been considered another important loss path. Indeed, the rate constants for the reactions of the C₁–C₄ aliphatic peroxy radicals and OH radicals have been measured experimentally.^{10–14} The very high rate constants show that the reaction with OH can be competitive to other reaction paths for peroxy radicals.^{15,16} Both theoretical and experimental studies of alkylperoxy radicals and OH reactions have shown that the main reaction channel is formation of ROOOH while the H-abstraction channel giving Criegee intermediate is to be of minor importance.^{14,17,18} However, the mechanism and kinetics for the reactions of aromatic peroxy radicals with OH radical are still unknown. Due to the effect of O₂-bridged bicyclic group substituent, the reactivity of aromatic peroxy radicals toward OH radical may be different. In this article, we apply density functional theory (DFT) and conventional transition-state theory (CTST) to investigate the reaction mechanisms and kinetics of the 1,3,5-TMB bicyclic peroxy radical (BPR) with OH radical.

2. Computational details

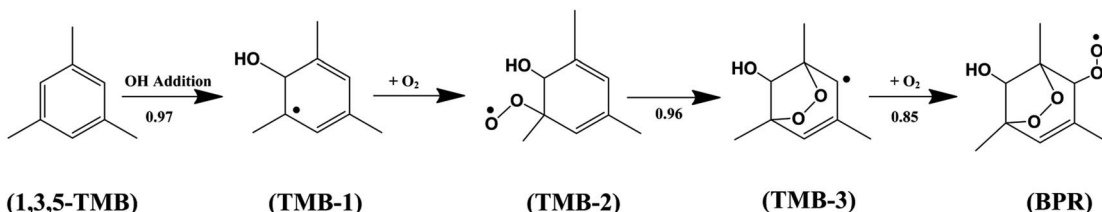
Modern quantum chemical calculations can obtain quantitative kinetics of atmospheric reactions,^{19–21} where quantitative accurate barrier heights are very key for obtaining quantitative rate constants. However, for the large and complex diradical reactions, it's particularly difficult to obtain quantitative barrier heights based on couple cluster theory. For example, the highly accurate CCSD(T) and CBS level can not obtain the quantitative barrier heights in the small-sized reaction of the simplest Criegee intermediate (CH₂O₂) with H₂O.¹⁹ Although post-CCSD(T) level of theory is able to deal with such radical–

^aLaboratory of Atmospheric Physico-Chemistry, Anhui Institute of Optics and Fine Mechanics, Chinese Academy of Sciences, Hefei, 230031, Anhui, China. E-mail: gaiyanbo@aiofm.ac.cn; wjzhang@aiofm.ac.cn

^bUniversity of Science and Technology of China, Hefei, 230026, Anhui, China

† Electronic supplementary information (ESI) available. See DOI: [10.1039/c9ra06562h](https://doi.org/10.1039/c9ra06562h)





Scheme 1

radical system, the computational costs are prohibitive. In contrast, the density functional theory (DFT) is the commonly used method in theoretical study on atmospheric oxidation of aromatic compounds.²²⁻²⁴ M08-HX hybrid functional shows excellent performance for thermochemistry, kinetics, non-covalent interactions.²⁵ Xu *et al.* carried out extensive systematic study on 48 transition state geometries of small reactions with a variety of methods.²⁶ It was found that M08-HX is the most highly recommended functional having a lower cost when compared to doubly hybrid functionals. Moreover, this method has been confirmed reliable by investigation of the small diradical reaction of CH_3O_2 and OH. The kinetic results show good agreement with the experimental values (see ESI† for details).

Thus, all stationary points including the reactants, reactant complexes, transition states and products on the potential energy surface of 1,3,5-TMB BPR + OH reaction have been fully optimized by the M08-HX functional with the 6-311 + g(2df,2p) basis set. Harmonic vibrational frequency computations were carried out at the same level in order to characterize the nature of the stationary points as either minima (all positive frequencies) or transition states (one and only one imaginary frequency), to provide the zero-point energies (ZPEs), and the thermodynamic contributions to the enthalpy and free energy. Besides, the intrinsic reaction coordinate (IRC)^{27,28} calculations were performed to ensure that the transition states connect the relevant reactants and products. The electronic structure and energy computations were carried out using the Gaussian 16 package.²⁹ The rate constants were calculated by conventional transition-state theory (CTST)³⁰⁻³² with the Eckart tunneling correction³³ using the TheRate program.^{34,35}

3 Results and discussion

The 1,3,5-TMB bicyclic peroxy radical can undergo both OH-addition and H-abstraction reactions. As shown in Scheme 2, the addition of OH radical to the terminal oxygen atom of the bicyclic peroxy radical forms a trioxide (ROOOH). Assaf *et al.*³⁶ suggested that for larger peroxy radicals with more than two or three C-atoms, the trioxide (ROOOH) intermediates undergo mostly collisional stabilization. Thus the ROOOH produced by OH addition on 1,3,5-TMB bicyclic peroxy radical is considered stabilized by collisional energy loss instead of prompt unimolecular reactions at atmospheric conditions. Different from the alkylperoxy radicals, there is a C=C double bond on the ring structure of the 1,3,5-TMB bicyclic peroxy radical. Thus the addition of the OH radical to the double bond to form OH-

adduct may also occur in the title reaction. In addition, the title reaction can be initiated through H-abstraction by OH radical to give Criegee intermediates which are mainly formed from the ozonolysis reaction of unsaturated substances^{37,38} due to the presence of CH group adjacent to the -OO' radical as shown in Scheme 3.

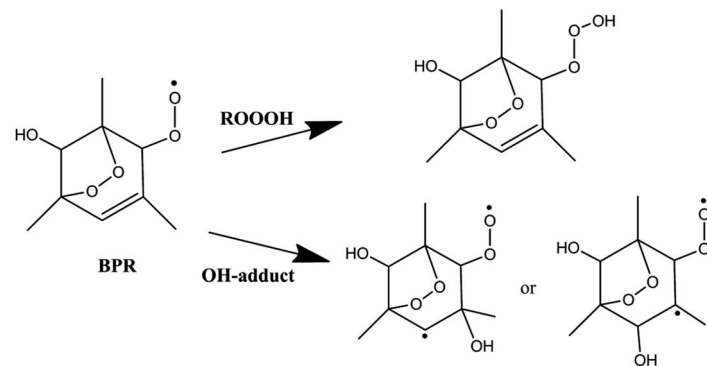
The schematic energy diagrams obtained at M08-HX/6-311+g(2df,2p) level of theory are displayed in Fig. 1. The most relevant geometrical parameters of all stationary points described in Fig. 1 have been drawn in Fig. 2. Table 1 presents the thermodynamic parameters including the relative energies ($\Delta(E + ZPE)$ and $\Delta E_{298\text{ K}}$), enthalpies ($\Delta H_{298\text{ K}}$), and Gibbs free energies ($\Delta G_{298\text{ K}}$). Then CTST rate constants of each channel at 298 K are listed in Table 2.

3.1. Trioxide formation between 1,3,5-TMB BPR and OH

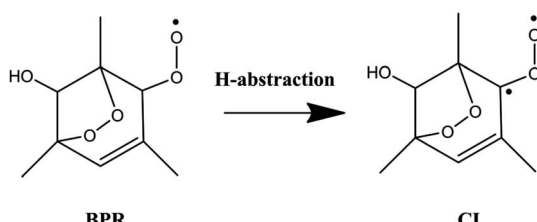
The important reaction between 1,3,5-TMB BPR and OH radical is addition of OH to the terminal oxygen atom of the peroxy end to produce ROOOH shown in Scheme 3. The large aromatic ROOOH is stabilized as Assaf *et al.*³⁶ predicted that the trioxide, ROOOH containing more than three carbons are nearly exclusively collisionally stabilized in atmospheric conditions. This reaction starts with a H-bonded reactant complex ${}^1\text{RC1}$ which is 4.14 kcal mol $^{-1}$ stabilized with respect to the separated reactants before the transition state ${}^1\text{TSA}$ and the corresponding product ROOOH, which is clearly displayed in Fig. 1. The structures of key species of the title reaction on the potential energy surface have been drawn in Fig. 2. In ${}^1\text{RC1}$ (see Fig. 2), the O···HO bonding occurs between the terminal O atom of BPR and the H atom of OH radical with the distance of 2.013 Å. In ${}^1\text{TSA}$, the vibration mode of the imaginary frequency shows reorientation of OH fragment and then addition to the terminal oxygen atom of the peroxy end forming a new O–O bond to give a trioxide, ROOOH. The formation of this trioxide is exothermic by 31.33 kcal mol $^{-1}$ in terms of $\Delta H_{298\text{ K}}$ (see Table 1). Seen from Fig. 1, the energy barrier of ${}^1\text{TSA}$ is computed to be –3.64 kcal mol $^{-1}$ with respect to the ${}^1\text{RC1}$ and the reactants, respectively, which is much lower than the energy barrier of ${}^1\text{TS1}$ (–0.46 kcal mol $^{-1}$) or ${}^3\text{TS1}$ (–1.19 kcal mol $^{-1}$).

3.2. OH-adduct formation between 1,3,5-TMB BPR and OH

As the 1,3,5-TMB BPR contains a double bond in the ring, the reaction of OH addition to the double bond producing OH-adduct should also be considered. Due to the substitution of the O₂-bridged group in 1,3,5-TMB BPR, the OH addition on the



Scheme 2



Scheme 3

C=C bond proceeds through a reactant complex (${}^3\text{RC2}$) by strong hydrogen bond interactions between the H from the OH radical and the O from the O_2 -bridged group (see Fig. 1 and 2).

The distances of the hydrogen bonds are 2.066 Å and 2.420 Å, and the binding energy of ${}^3\text{RC2}$ is $-7.47 \text{ kcal mol}^{-1}$. Then the reaction continues by addition of the OH radical to either of the carbon atoms of the double bond through the triplet transition states ${}^3\text{TSA1}$ and ${}^3\text{TSA2}$. Due to this addition, the OH-adduct 1 is formed by a shortening of C···OH bond from 2.060 Å in ${}^3\text{TSA1}$ to 1.427 Å, simultaneously, the C=C bond length is elongated from 1.358 Å in ${}^3\text{TSA1}$ to 1.496 Å in the product OH-adduct 1. Similarly, the OH-adduct 2 is formed by a shortening of C···OH bond from 2.062 Å in ${}^3\text{TSA2}$ to 1.414 Å, at the same time, the C=C bond length is elongated from 1.356 Å in ${}^3\text{TSA2}$ to 1.497 Å in the product OH-adduct 2. The formation of OH-adduct 1 and OH-adduct 2 are exothermic by 32.52 and 34.91 kcal mol^{-1}

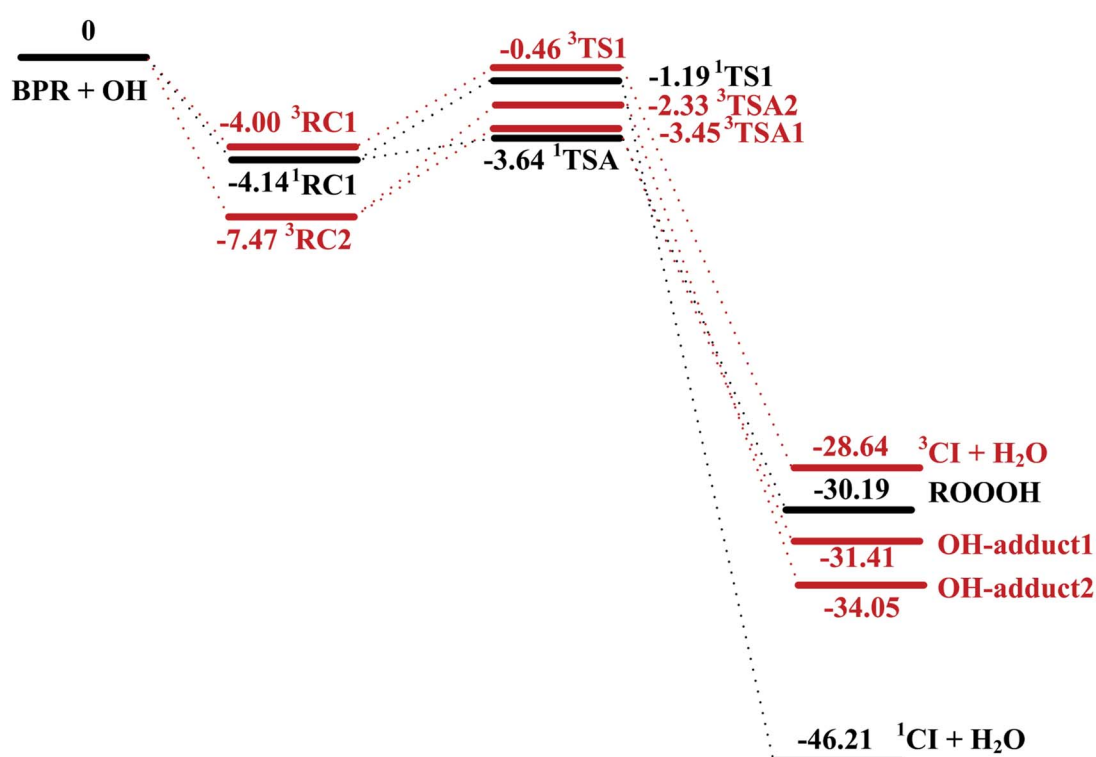


Fig. 1 Potential energy surface for BPR + OH biradical reactions. The energies (kcal mol^{-1}) relative to separated reactants BPR and OH at M08-HX/6-311 + g(2df,2p) level of theory. RC, reactant complex; TS, transition state; CI, Criegee intermediate. The singlet reaction pathways are depicted in black, and the triplet reaction pathways are depicted in red for clarity.



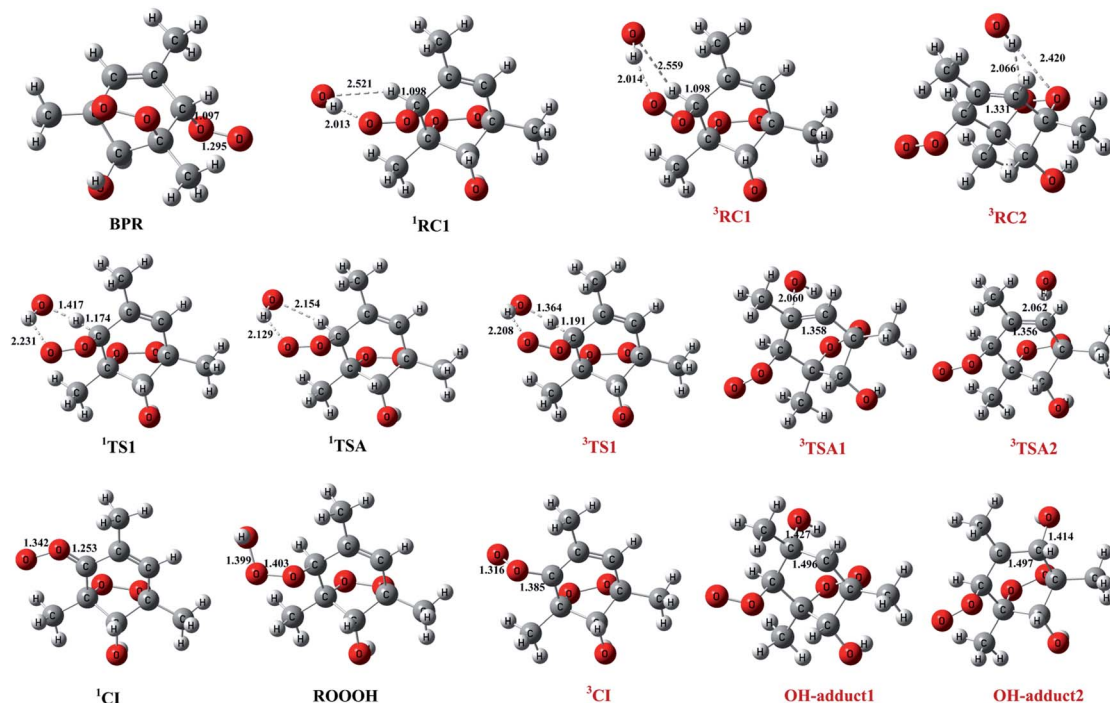


Fig. 2 Structures of key species in the reaction of bicyclic peroxy radical (BPR) with OH optimized at M08-HX/6-311 + g(2df,2p) level of theory. The singlet species are named in black, while the triplet ones are named in red for clarity. Bond distances are in angstrom.

respectively in terms of $\Delta H_{298\text{ K}}$ (see Table 1). The energy barriers of $^3\text{TSA1}$ and $^3\text{TSA2}$ are $-3.45\text{ kcal mol}^{-1}$ and $-2.33\text{ kcal mol}^{-1}$ respectively, which are also lower than that of $^1\text{TS1}$ or $^3\text{TS1}$, indicating that OH addition reactions including the formation of ROOOH and OH-adducts are the dominant pathways. This conclusion can be supported by the study of kinetics in the following section.

3.3. Criegee intermediate formation between 1,3,5-TMB BPR and OH

The hydrogen abstraction reaction of 1,3,5-TMB bicyclic peroxy radical with OH to form Criegee intermediate can occur *via* both singlet and triplet potential energy surfaces (PESs). On the singlet PES, as shown in Fig. 1, the H-abstraction pathway starts with the reactant complex $^1\text{RC1}$. Thereafter, $^1\text{RC1}$ is transformed into ^1CI and water through a transition state $^1\text{TS1}$ with the energy barrier of $-1.19\text{ kcal mol}^{-1}$ (with respect to the reactants). In $^1\text{TS1}$, the C-H bond is breaking with the distance of 1.174 \AA . Simultaneously, the H atom is abstracted by the O atom from OH with the bond length of 1.417 \AA . In addition, this reaction producing singlet CI (^1CI) is significantly exothermic ($\Delta H_{298\text{ K}} = -46.19\text{ kcal mol}^{-1}$, see Table 1). The H-abstraction mechanism is also found on the triplet PES. As shown in Fig. 1, the initial step is formation of a reactant complex $^3\text{RC1}$ stabilized by $4.00\text{ kcal mol}^{-1}$ with respect to the reactants. As seen from Fig. 2, the $^3\text{RC1}$ is characterized by H-bond interaction with the bond length of 2.014 \AA between the hydrogen atom of OH and the terminal oxygen atom of BPR. Then the H atom of BPR is abstracted by OH radical, leading to the formation of ^3CI + H_2O *via* $^3\text{TS1}$. This transition state $^3\text{TS1}$ is lower located than

the reactants by $0.46\text{ kcal mol}^{-1}$ which involves a shortening of $\text{H}\cdots\text{OH}$ bond (from 2.559 to 1.364 \AA) and an elongation of the C-H bond (from 1.098 to 1.191 \AA) which will eventually break. Additionally, this reaction producing triplet CI (^3CI) is moderately exothermic ($\Delta H_{298\text{ K}} = -28.09\text{ kcal mol}^{-1}$, see Table 1).

As seen from Fig. 2, the singlet $^1\text{RC1}$ and triplet $^3\text{RC1}$, as well as the corresponding $^1\text{TS1}$ and triplet $^3\text{TS1}$ all show six-membered ring forms though there are some structural discrepancies in the reactant complexes and transition states. The energy barrier of $^1\text{TS1}$ and $^3\text{TS1}$ differs by $0.73\text{ kcal mol}^{-1}$,

Table 1 Relative energies ($\Delta(E + \text{ZPE})$ and $\Delta E_{298\text{ K}}$), enthalpies ($\Delta H_{298\text{ K}}$), and Gibbs free energies ($\Delta G_{298\text{ K}}$) for the BPR + OH reaction. All energies are calculated relative to the energy of BPR + OH, in units of kcal mol^{-1} , at the M08-HX/6-311 + g(2df,2p) level of theory

Compound	$\Delta(E + \text{ZPE})$	$\Delta E_{298\text{ K}}$	$\Delta H_{298\text{ K}}$	$\Delta G_{298\text{ K}}$
BPR + OH	0	0	0	0
$^1\text{RC1}$	-4.14	-3.92	-4.51	4.53
$^1\text{TS1}$	-1.19	-1.44	-2.04	8.30
$^1\text{CI} + \text{H}_2\text{O}$	-46.21	-46.19	-46.19	-45.86
^1TSA	-3.64	-3.77	-4.36	5.65
ROOOH	-30.19	-30.74	-31.33	-20.17
$^3\text{RC1}$	-4.00	-3.85	-4.44	4.10
$^3\text{TS1}$	-0.46	-0.65	-1.24	8.19
$^3\text{CI} + \text{H}_2\text{O}$	-28.64	-28.09	-28.09	-30.01
$^3\text{RC2}$	-7.47	-7.15	-7.74	0.60
$^3\text{TSA1}$	-3.45	-3.82	-4.41	5.77
OH-adduct 1	-31.41	-31.93	-32.52	-21.84
$^3\text{TSA2}$	-2.33	-2.58	-3.17	6.48
OH-adduct 2	-34.05	-34.32	-34.91	-25.62



Table 2 Calculated values at 298 K of equilibrium constants (K_{eq} , $\text{cm}^3 \text{ mol}^{-1}$), the Eckart tunneling correction (κ), unimolecular rate constants (k_2 , s^{-1}) including tunneling correction, rate constants (k_{TS} , $\text{cm}^3 \text{ mol}^{-1} \text{ s}^{-1}$), and the overall rate constant k_{Total} ($k_{\text{Total}} = k_{^1\text{TS}1} + k_{^1\text{TSA}} + k_{^3\text{TS}1} + k_{^3\text{TSA}1} + k_{^3\text{TSA}2}$, $\text{cm}^3 \text{ mol}^{-1} \text{ s}^{-1}$)

Reaction pathways	K_{eq}	κ	k_2	k_{TS}	k_{Total}
$^1\text{TS}1$	1.95×10^{-23}	2.10	2.23×10^{10}	4.35×10^{-13}	5.01×10^{-11}
^1TSA	1.95×10^{-23}	1.02	9.62×10^{11}	1.88×10^{-11}	
$^3\text{TS}1$	4.02×10^{-23}	2.52	1.57×10^{10}	6.31×10^{-13}	
$^3\text{TSA}1$	1.49×10^{-20}	1.56	1.55×10^9	2.31×10^{-11}	
$^3\text{TSA}2$	1.49×10^{-20}	1.60	4.81×10^8	7.17×10^{-12}	

indicating that, for the hydrogen abstraction mechanism, the reaction rate of singlet Criegee intermediate ^1CI formation is close to that of triplet ^3CI formation.

3.4. Kinetics

It has been shown that either OH addition or H-abstraction pathway consists of a reversible first step involving the barrierless formation of a reactant complex (RC), followed by the irreversible formation of products. Therefore, the reaction pathway is a two-step process as described by Scheme 4, where the reactant complex is in equilibrium with the reactants.

If k_1 and k_{-1} are the rate constants for the first step and k_2 is the rate constant for the second, a steady-state analysis leads to a rate constant for the reaction pathway under consideration, which can be approximated as

$$k = \frac{k_1}{k_{-1}} k_2 = K_{\text{eq}} k_2 \quad (1)$$

where K_{eq} stands for the equilibrium constant in the first step, which can be written as

$$K_{\text{eq}} = \frac{Q_{\text{RC}}}{Q_{\text{R}}} e^{-(E_{\text{RC}} - E_{\text{R}})/(RT)} \quad (2)$$

According to the conventional transition state theory, the unimolecular rate constant k_2 with the Eckart tunneling correction is given by

$$k_2 = \sigma \kappa \frac{k_B T}{h} \frac{Q_{\text{TS}}^{\neq}}{Q_{\text{RC}}} e^{-(E_{\text{TS}} - E_{\text{RC}})/(RT)} \quad (3)$$

where Q_{TS}^{\neq} , Q_{R} and Q_{RC} are partition functions of the transition state, the reactants and the reactant complex, σ is the symmetry factor, κ is the tunneling factor, k_B is the Boltzmann's constant, and h is Planck's constant. The E_{TS} , E_{R} and E_{RC} are the total energy inclusion ZPE correction of the transition state, the reactants and the reactant complex.

The rate coefficients were calculated using the M08-HX/6-311 + g(2df,2p) optimized geometrical parameters, frequencies and

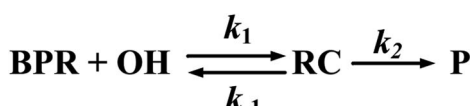
energies listed in Table 2. From Table 2, the rate constants of OH addition reactions by ^1TSA , $^3\text{TSA}1$ and $^3\text{TSA}2$ are computed to be $1.88 \times 10^{-11} \text{ cm}^3 \text{ mol}^{-1} \text{ s}^{-1}$, $2.31 \times 10^{-11} \text{ cm}^3 \text{ mol}^{-1} \text{ s}^{-1}$, and $7.17 \times 10^{-12} \text{ cm}^3 \text{ mol}^{-1} \text{ s}^{-1}$ respectively. While the rate constants of H-abstractions *via* singlet $^1\text{TS}1$ and triplet $^3\text{TS}1$ at 298 K are $4.35 \times 10^{-13} \text{ cm}^3 \text{ mol}^{-1} \text{ s}^{-1}$ and $6.31 \times 10^{-13} \text{ cm}^3 \text{ mol}^{-1} \text{ s}^{-1}$ respectively. The computed overall rate constant is $5.01 \times 10^{-11} \text{ cm}^3 \text{ mol}^{-1} \text{ s}^{-1}$. The atmospheric lifetime of the studied 1,3,5-trimethylbenzene bicyclic peroxy radical due to reaction with OH can be estimated to be 5.54 hour using the following expression: $\tau = 1/[k[X]]$, where X is the average concentration of OH in the atmosphere ($[\text{OH}] = 1.0 \times 10^6$ molecules per cm^{-3}).³⁹ The branching ratios for H-abstraction pathways *via* $^1\text{TS}1$ and $^3\text{TS}1$ are only 8.68×10^{-3} and 1.26×10^{-2} respectively. Hence the OH addition reactions including the formation of ROOOH and OH-adducts are the major paths in contrast with H-abstraction channels producing Criegee intermediate which are negligible. The degradation of the ROOOH species in the atmosphere is significant which might help explain the difference in simulated and observed OH concentrations under low NOx environment.⁴⁰ The OH-adducts may contribute to the formation and growth of SOA through subsequent reactions. Therefore, research is urgently needed into the atmospheric fate and possible influence of the 1,3,5-TMB ROOOH and OH-adducts on atmospheric chemistry.

4. Conclusions

In the present study, the mechanism and kinetics of the atmospheric reaction of 1,3,5-TMB bicyclic peroxy radical with OH have been studied by M08-HX/6-311 + g(2df,2p) method and CTST including Eckart tunneling correction. The conclusions are drawn in the following:

(1) Two types of mechanisms including OH addition producing ROOOH and OH-adducts, and H-abstraction for Criegee intermediate formation are considered. Both the OH addition to the peroxy end and to the double bond of 1,3,5-TMB bicyclic peroxy radical are easier than H-abstraction reaction due to the lower energy barrier.

(2) The rate constants of OH addition to BPR are computed to be $1.88 \times 10^{-11} \text{ cm}^3 \text{ mol}^{-1} \text{ s}^{-1}$, $2.31 \times 10^{-11} \text{ cm}^3 \text{ mol}^{-1} \text{ s}^{-1}$, and $7.17 \times 10^{-12} \text{ cm}^3 \text{ mol}^{-1} \text{ s}^{-1}$ by ^1TSA , $^3\text{TSA}1$ and $^3\text{TSA}2$ respectively, while the abstraction rate constants *via* $^1\text{TS}1$ and $^3\text{TS}1$ are calculated to be $4.35 \times 10^{-13} \text{ cm}^3 \text{ mol}^{-1} \text{ s}^{-1}$ and $6.31 \times 10^{-13} \text{ cm}^3 \text{ mol}^{-1} \text{ s}^{-1}$ respectively at 298 K. Kinetically, the abstraction



Scheme 4



reactions are much less favorable than OH-addition reactions, thus can be negligible.

(3) The 1,3,5-TMB ROOOH and OH-adducts are the most dominant products. The atmospheric fate and possible influence of the ROOOH and OH-adducts on atmospheric chemistry have not been explored yet.

Conflicts of interest

There are no conflicts to declare.

Acknowledgements

We would like to thank financial support from the National Natural Science Foundation of China (41605102, 91544228, 41575125, 21876177, 41775125), the National Key Research and Development Program of China (2016YFC0202205, 2017YFC0209401), the Youth Innovation Promotion Association CAS (2019439), and the Science and Technology Foundation of Guizhou Province, China ([2019]5648 and [2018]1080).

References

- 1 R. G. Derwent, T. J. Davies, M. Delaney, G. J. Dollard, R. A. Field, P. Dumitresan, P. D. Nason, B. M. R. Jones and S. A. Pepler, *Atmos. Environ.*, 2000, **34**, 297–312.
- 2 L. T. Molina, C. E. Kolb, B. de Foy, B. K. Lamb, W. H. Brune, J. L. Jimenez, R. Ramos-Villegas, J. Sarmiento, V. H. Paramo-Figueroa, B. Cardenas, V. Gutierrez-Avedoy and M. J. Molina, *Atmos. Chem. Phys.*, 2007, **7**, 2447–2473.
- 3 E. Velasco, B. Lamb, H. Westberg, E. Allwine, G. Sosa, J. L. Arriaga-Colina, B. T. Jobson, M. L. Alexander, P. Prazeller, W. B. Knighton, T. M. Rogers, M. Grutter, S. C. Herndon, C. E. Kolb, M. Zavala, B. de Foy, R. Volkamer, L. T. Molina and M. J. Molina, *Atmos. Chem. Phys.*, 2008, **7**, 329–353.
- 4 A. Metzger, J. Dommen, K. Gaeggeler, J. Duplissy, A. S. H. Prevot, J. Kleffmann, Y. Elshorbany, A. Wisthaler and U. Baltensperger, *Atmos. Chem. Phys.*, 2008, **8**, 6453–6468.
- 5 M. J. Elrod, *J. Phys. Chem. A*, 2011, **115**, 8125–8130.
- 6 K. P. Wyche, P. S. Monks, A. M. Ellis, R. L. Cordell, A. E. Parker, C. Whyte, A. Metzger, J. Dommen, J. Duplissy, A. S. H. Prevot, U. Baltensperger, A. R. Rickard and F. Wulfert, *Atmos. Chem. Phys.*, 2009, **9**, 635–665.
- 7 M. E. Jenkin and K. C. Clemitsshaw, *Atmos. Environ.*, 2000, **34**, 2499–2527.
- 8 J. J. Orlando and G. S. Tyndall, *Chem. Soc. Rev.*, 2012, **41**, 6294–6317.
- 9 J. A. Thornton, P. J. Wooldridge, R. C. Cohen, M. Martinez, H. Harder, W. H. Brune, E. J. Williams, J. M. Roberts, F. C. Fehsenfeld, S. R. Hall, R. E. Shetter, B. P. Wert and A. Fried, *J. Geophys. Res.*, 2002, **107**, ACH 7-1–ACH 7-17.
- 10 E. Assaf, B. Song, A. Tomas, C. Schoemaecker and C. Fittschen, *J. Phys. Chem. A*, 2016, **120**, 8923–8932.
- 11 E. Assaf, S. Tanaka, Y. Kajii, C. Schoemaecker and C. Fittschen, *Chem. Phys. Lett.*, 2017, **684**, 245–249.
- 12 A. Bossolasco, E. P. Faragó, C. Schoemaecker and C. Fittschen, *Chem. Phys. Lett.*, 2014, **593**, 7–13.
- 13 E. P. Faragó, C. Schoemaecker, B. Viskolcz and C. Fittschen, *Chem. Phys. Lett.*, 2015, **619**, 196–200.
- 14 C. Yan, S. Kocevska and L. N. Krasnoperov, *J. Phys. Chem. A*, 2016, **120**, 6111–6121.
- 15 A. T. Archibald, A. S. Petit, C. J. Percival, J. N. Harvey and D. E. Shallcross, *Atmos. Sci. Lett.*, 2009, **10**, 102–108.
- 16 C. Fittschen, L. K. Whalley and D. E. Heard, *Environ. Sci. Technol.*, 2014, **48**, 7700–7701.
- 17 E. Assaf, L. Sheps, L. Whalley, D. Heard, A. Tomas, C. Schoemaecker and C. Fittschen, *Environ. Sci. Technol.*, 2017, **51**, 2170–2177.
- 18 J. F. Müller, Z. Liu, V. S. Nguyen, T. Stavrakou, J. N. Harvey and J. Peeters, *Nat. Commun.*, 2016, **7**, 13213.
- 19 B. Long, J. L. Bao and D. G. Truhlar, *J. Am. Chem. Soc.*, 2016, **138**, 14409–14422.
- 20 B. Long, J. L. Bao and D. G. Truhlar, *Proc. Natl. Acad. Sci. U. S. A.*, 2018, **115**, 6135–6140.
- 21 B. Long, J. L. Bao and D. G. Truhlar, *J. Am. Chem. Soc.*, 2019, **141**, 611–617.
- 22 M. Altarawneh, E. M. Kennedy, B. Z. Dlugogorski and J. C. Mackie, *J. Phys. Chem. A*, 2008, **112**, 6960–6967.
- 23 T. J. Frankcombe, *J. Phys. Chem. A*, 2008, **112**, 1572–1575.
- 24 J. M. Andino, J. N. Smith, R. C. Flagan, W. A. Goddard and J. H. Seinfeld, *J. Phys. Chem.*, 1996, **100**, 10967–10980.
- 25 Y. Zhao and D. G. Truhlar, *J. Chem. Theory Comput.*, 2008, **4**, 1849–1868.
- 26 X. F. Xu, I. M. Alecu and D. G. Truhlar, *J. Chem. Theory Comput.*, 2011, **7**, 1667–1676.
- 27 C. Gonzalez and H. B. Schlegel, *J. Phys. Chem.*, 1989, **90**, 2154–2161.
- 28 C. Gonzalez and H. B. Schlegel, *J. Phys. Chem.*, 1990, **94**, 5523–5527.
- 29 M. J. Frisch, G. W. Trucks, H. B. Schlegel, G. E. Scuseria, M. A. Robb, J. R. Cheeseman, G. Scalmani, V. Barone, G. A. Petersson, H. Nakatsuji, X. Li, M. Caricato, A. V. Marenich, J. Bloino, B. G. Janesko, R. Gomperts, B. Mennucci, H. P. Hratchian, J. V. Ortiz, A. F. Izmaylov, J. L. Sonnenberg, D. Williams-Young, F. Ding, F. Lipparini, F. Egidi, J. Goings, B. Peng, A. Petrone, T. Henderson, D. Ranasinghe, V. G. Zakrzewski, J. Gao, N. Rega, G. Zheng, W. Liang, M. Hada, M. Ehara, K. Toyota, R. Fukuda, J. Hasegawa, M. Ishida, T. Nakajima, Y. Honda, O. Kitao, H. Nakai, T. Vreven, K. Throssell, J. A. Montgomery Jr, J. E. Peralta, F. Ogliaro, M. J. Bearpark, J. J. Heyd, E. N. Brothers, K. N. Kudin, V. N. Staroverov, T. A. Keith, R. Kobayashi, J. Normand, K. Raghavachari, A. P. Rendell, J. C. Burant, S. S. Iyengar, J. Tomasi, M. Cossi, J. M. Millam, M. Klene, C. Adamo, R. Cammi, J. W. Ochterski, R. L. Martin, K. Morokuma, O. Farkas, J. B. Foresman, and D. J. Fox, *Gaussian 16, Revision A.03*, Gaussian, Inc., Wallingford CT, 2016.
- 30 M. G. Evans and M. Polanyi, *Trans. Faraday Soc.*, 1935, **31**, 875–894.
- 31 H. Eyring, *J. Chem. Phys.*, 1935, **3**, 107–115.



32 D. G. Truhlar, B. C. Garrett and S. J. Klippenstein, *J. Phys. Chem.*, 1996, **100**, 12771–12800.

33 C. Eckart, *Phys. Rev.*, 1930, **35**, 1303–1309.

34 W. T. Duncan, R. L. Bell and T. N. Truong, *J. Comput. Chem.*, 1998, **19**, 1039–1052.

35 S. Zhang and T. N. Truong, *VKLabs*, version 1.0. University of Utah: Salt Lake City, UT, 2001.

36 E. Assaf, C. Schoemaecker, L. Vereecken and C. Fittschen, *Int. J. Chem. Kinet.*, 2018, **50**, 670–680.

37 M. A. H. Khan, C. J. Percival, R. L. Caravan, C. A. Taatjesc and D. E. Shallcross, *Environ. Sci.: Processes Impacts*, 2018, **20**, 437–453.

38 D. Osborn and C. A. Taatjesc, *Int. Rev. Phys. Chem.*, 2015, **34**, 309–360.

39 W. J. Bloss, M. J. Evans, J. D. Lee, R. Sommariva, D. E. Heard and M. J. Pilling, *Faraday Discuss.*, 2005, **130**, 425–436.

40 C. Fittschen, M. A. Ajami, S. Batut, V. Ferracci, S. Archer-Nicholls, A. T. Archibald and C. Schoemaecker, *Atmos. Chem. Phys.*, 2019, **19**, 349–362.

